Scanning Tunneling Microscopy of Layered Molecular Conductors

Michael A. Dvorak, Shulong Li, and Michael D. Ward*

Department of Chemical Engineering and Materials Science, University of Minnesota, Amundson Hall, 421 Washington Ave. S.E., Minneapolis, Minnesota 55455

Received February 2, 1994. Revised Manuscript Received March 21, 1994®

Scanning tunneling microscopy (STM) of single crystals of semiconducting organic crystalline charge-transfer salts $[R_1(R_2)\overline{NCH_2CH_2OCH_2CH_2}]^+[TCNQ]_2^-$ (**1a**: $R_1 = C_2H_5$, $R_2 = C_2H_5$; **1b**: $R_1 = CH_3$, $R_2 = C_2H_5$; **1c**: $R_1 = CH_3$, $R_2 = CH_3$, monoclinic; **1d**: $R_1 = CH_3$, $R_2 = CH_3$, triclinic) and $(Ph(H)NCH{=}CHCH{=}N(H)Ph)^+(TCNQ)_2^-$ (TCNQ = tetracyanoquinodimethane) is described. The STM data reveal tunneling current features that compare favorably with the electronic properties and crystal structure of the salts. The local density of states (LDOS) exhibit orientation and corrugation consistent with the topography and electronic structure of dimerized TCNQ stacks contained in the molecular layers that define the exposed low-energy crystal planes. In the case of **1a**, crystallographically inequivalent TCNQ layers that alternate through the crystal are revealed in STM data by sequential etching of the layers. The two dimorphs **1c** and **1d** reveal dramatically different tunneling current contrast due to the different molecular motifs of their respective crystal faces, as surmised from the crystal structure. While the lattice constants determined from the tunneling current contrast correspond favorably with the values expected based on single-crystal X-ray structures, in some cases there appears to be a slight compression of the surface layer. This behavior is consistent with weak interaction between the molecular layers of the charge-transfer salt, and the tendency of the molecular constituents in the surface layer to achieve a higher packing density in order to lower the crystal surface free energy. These studies reveal that STM can provide substantial insight into the structure of organic crystals, and can probe molecular-level structural and electronic features.

Introduction

Crystalline solids based on molecular components exhibit numerous electronic phenomena, including electrical conductivity, superconductivity, nonlinear optical behavior, and ferromagnetism.[1-4] The most extensively examined molecular crystals have been the low-dimensional conductors and semiconductors, which generally exhibit anisotropic conductivity due to extended band structure associated with stacks of open-shell charge-transfer molecules. Most notable are the organic superconductors and ferromagnetic materials based on metallocene salts of polycyanoanions. The principle advantage of molecular materials is the ability to rationally control bulk properties through molecular design. Further advances in this area, however, require a thorough understanding of the relationship between molecular structure, supramolecular structure, and electronic properties. Better understanding of the *surface* topographical and electronic structure of these materials is also needed in order to provide insight into their nucleation and growth characteristics, particularly with regard to crystal size, morphology, growth orientation, and defect density. We have been particularly interested in the mechanisms of nucleation and growth of organic crystals on the nanoscopic level, where topographic features such as terraces, ledges, and kinks play an important role in these processes.[5] This has required a detailed understanding of the distribution of these features, their relationship to the directionality and strength of intermolecular interactions, and the degree of reconstruction of exposed crystal faces compared to the bulk structure.

These needs have prompted us to examine conducting molecular crystals with scanning tunneling microscopy (STM).[6] This technique is particularly suited to examining the relationship of the electronic and molecular structure of specific crystal planes to the bulk material, as well as characterizing the microscopic topography of crystal surfaces. The tunneling current, i_T, measured in STM provides a contour of the density of states, $\rho(r,E_F)$, that reflects the molecular and electronic structure associated with molecular constituents in the crystal plane under

* To whom correspondence should be addressed.

® Abstract published in *Advance ACS Abstracts*, August 15, 1994.

(1) (a) Lehn, J.-M. *Angew. Chem., Int. Ed. Engl.* **1988**, *27*, 89. (b) *Molecular Electronic Devices*; Carter, F. L., Ed.; Marcel Dekker, New York, 1982. (c) *Extended Linear Chain Compounds*; Miller, J. S., Ed.; Plenum, New York, 1982-1983; Vols. 1-3. (d) Desiraju, G. *Crystal Engineering*; Elsevier, New York, 1989. (e) Miller, J. S.; Epstein, A. J.; Reiff, W. M. *Science* **1988**, *240*, 40.

(2) (a) *Nonlinear Optical Properties of Organic Molecules and Crystals*; Chemla, D. S., Zyss, J., Eds.; Academic Press: Orlando, FL, 1987; Vol. 1.

(3) (a) Williams, J. M.; Carneiro, K. *Adv. Inorg. Chem. Radiochem.* **1985**, *29*, 249. (b) Inokuchi, H. *Angew. Chem., Int. Ed. Engl.* **1988**, *27*, 1747. (c) Emge, T. J.; Leung, P. C. W.; Beno, M. A.; Wang, H. H.; Firestone, M. A.; Webb, K. S.; Carlson, K. D.; Williams, J. M.; Venturini, E. L.; Azevedo, L. J.; Schirber, J. E. *Mol. Cryst. Liq. Cryst.* **1986**, *132*, 363. (d) Montgomery, L. K.; Geiser, U., Wang, H. H.; Beno, M. A.; Schultz, A. J.; Kini, A. M.; Carlson, K. D.; Williams, J. M.; Whitworh, J. R. *Synth. Met.* **1988**, *27*, A195.

(4) (a) Miller, J. S.; Epstein, A. J.; Reiff, W. M. *Acc. Chem. Res.* **1988**, *21*, 114. (b) Miller, J. S.; Epstein, A. J.; Reiff, W. M. *Science* **1988**, *240*, 40.

(5) (a) Carter, P. W.; Ward, M. D. *J. Am. Chem. Soc.* **1993**, *115*, 11521. (b) Carter, P. W.; Hillier, A. C.; Ward, M. D. *J. Am. Chem. Soc.* **1994**, *116*, 944. (c) Hillier, A. C.; Ward, M. D. *Science* **1994**, *263*, 1261.

(6) (a) Binnig, G.; Rohrer, H.; Gerber, Ch.; Weibel, E. *Phys. Rev. Lett.* **1982**, *49*, 57. (b) Spong, J. K.; Mizes, H. A.; LaComb, L. J.; Dovek, M. M.; Frommer, J. E.; Foster, J. S. *Nature* **1989**, *338*, 137. (c) Smith, D. P. E.; Horber, H.; Gerber, Ch.: Binnig, G. *Science* **1989**, *245*, 43. (d) Binning, G.; Quate, C. F.; Gerber, Ch. *Phys. Rev. Lett.* **1986**, *56*, 930.

0897-4756/94/2806-1386$04.50/0

Chart 1

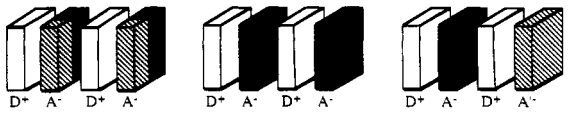

inequivalent TCNQ stacks in the same layer
$[(\eta\text{-}C_5Me_5)_2Ru(\eta^6,\eta^6\text{-}[2_2](1,4)\text{-cyclophane})]^{2+}[TCNQ]_4^{2-}$

equivalent TCNQ stacks equivalent layers
1b, 1c,1d

inequivalent TCNQ stacks in inequivalent layers
1a, 2

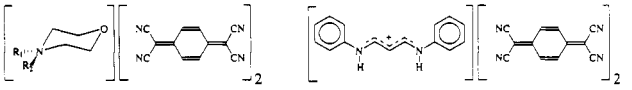

(morpholinium)$^+$(TCNQ)$_2^-$
1a: $R_1 = C_2H_5$; $R_2 = C_2H_5$
1b: $R_1 = CH_3$; $R_2 = C_2H_5$
1c: $R_1 = CH_3$; $R_2 = CH_3$ (monoclinic)
1d: $R_1 = CH_3$; $R_2 = CH_3$ (triclinic)

(vinamidinium)$^+$(TCNQ)$_2^-$
2

investigation. Recently, STM has been used to examine the electronic structure of several low dimensional inorganic conductors[7,8] and superconductors,[9] as well as organic charge-transfer salts based on bis(ethylenedithiotetrathiafulvalene),[10] tetramethyltetraselenafulvalene,[11] tetrathiafulvalenium, and tetracyanoquinodimethane.[12,13]

Our recent STM investigations of single crystals of the molecular semiconductor $[(\eta\text{-}C_5Me_5)_2Ru(\eta^6,\eta^6\text{-}[2_2](1,4)\text{-cyclophane})^{2+}[TCNQ]_4^{2-}$ (TCNQ = tetracyanoquinodimethane) demonstrated that STM was capable of distinguishing independent electronic subsystems, in the form of charge density waves associated with crystallographically inequivalent TCNQ anion stacks (A^-). These stacks coexisted in molecular TCNQ layers separated by cation (D^+) layers (Chart 1).[13a] This ability to probe electronic structure on a molecular level prompted us to examine further the organic crystalline charge-transfer salts based on morpholinium ($MORPH^+$) and vinamidinium (VIN^+) cations, and TCNQ anions, with the composition $[R_1(R_2)\overline{NCH_2CH_2OCH_2CH_2}]+[TCNQ]_2^-$ (**1a**: $R_1 = C_2H_5$, $R_2 = C_2H_5$; **1b**: $R_1 = CH_3$, $R_2 = C_2H_5$; **1c**: $R_1 = CH_3$, $R_2 = CH_3$, monoclinic; **1d**: $R_1 = CH_3$, $R_2 = CH_3$, triclinic) and $(Ph(H)NCH{=}CHCH{=}N(H)Ph)^+(TCNQ)_2^-$ (**2**). These materials possess extended TCNQ stacks, the 1:2 stoichiometry dictating an average charge of $\rho = 0.5-$ per TCNQ site.[14] These features result in anisotropic conductivity and semiconducting behavior, typical of low dimensional TCNQ solids. Each of these compounds possess TCNQ stacks organized into discrete molecular layers, which are separated by layers of cations. These layers, because of strong intermolecular in-plane interactions, tend to form large, molecularly flat crystal faces which are amenable to STM investigations. Notably, these compounds differ with respect to the crystallographic equivalence of the TCNQ layers: **1a** and **2** each have two crystallographically inequivalent TCNQ stacks organized into two separate crystallographically inequivalent layers, whereas **1b–d** possess crystallographically equivalent layers. The diversity of molecular motifs evident in these charge-transfer salts provides an opportunity to examine the relationship between well-defined bulk structural and electronic structure and $\rho(r,E_F)$. We report herein STM investigations of these salts, which demonstrate the relationship between tunneling characteristics and the molecular and electronic structure of these charge-transfer salts.

Experimental Section

Materials. Single crystals of $(MORPH)^+(TCNQ)_2^-$ salts (**1a–d**) were grown by slow cooling of acetonitrile solutions containing stoichiometric amounts of TCNQ and the appropriate $(MORPH)^+I^-$ salt. $(VIN)^+(TCNQ)_2^-$ (**2**) was prepared in a similar manner, from the $(VIN)^+I^-$ salt, which was synthesized according to a previously described method.[15] Crystals typically had dimensions of 3 mm × 3 mm × 0.5 mm; the largest faces were chosen for investigation by STM. Freshly prepared crystals were used as grown, whereas crystals that had been left standing in ambient air were cleaned occasionally (i.e., once per week) by immersion in a neat acetonitrile solution. No appreciable differences were observed between freshly prepared and aged crystals. All crystals were indexed with a Enraf-Nonius CAD4 computer-controlled X-ray diffractometer in order to assign the crystal faces.

Apparatus. A Nanoscope II scanning tunneling microscope, with 80% Pt/20% Ir mechanically cut tips, was used to obtain all images. Each crystal specimen was placed on a conductive sheet of aluminum and secured to the STM fixture with either strips of adhesive tape or silver epoxy. The crystals were affixed to the stage after indexing, so that their crystallographic orientation under the STM tip was known. The scanning conditions involved tip bias voltages ranging from −200 to −1700 mV (tip vs sample) with setpoint currents ranging from 0.10 to 0.55 nA. All images shown here were collected in the constant-height mode. Crystal structure data were obtained from the Cambridge Structural Database, Cambridge Crystallographic Data Centre, University Chemical Library, Cambridge England, Version 5.05, update April 1993.

Results

The contour of the density of states, $\rho(r,E_F)$, obtained from STM data is a consequence of the surface topography, molecular structure, and electronic states near the Fermi level. Accordingly, the orientation, shape, dimension, and

(7) (a) Lieber, C. M.; Wu, X. L. *Acc. Chem. Res.* **1991**, *24*, 170. (b) Parkinson, B. A. *J. Am. Chem. Soc.* **1991**, *113*, 7833.

(8) (a) Coleman, R. V.; Giambattista, B.; Hansma, P. K.; Johnson, A.; McNairy, W. W.; Slough, C. G. *Adv. Phys.* **1988**, *37*, 559. (b) Tang, S. L.; Kasowski, R. V.; Parkinson, B. A. *Phys. Rev. B* **1989**, *39*, 9987. (c) Tang, S. L.; Kasowski, R. V.; Suna, A.; Parkinson, B. A. *Surf. Sci.* **1991**, *238*, 280. (d) Wang, C.; Giambattista, B.; Slough, C. G.; Coleman, R. V. *Phys. Rev. B* **1990**, *42*, 8890. (e) Slough, C. G.; McNairy, W. W.; Coleman, R. V.; Garnaes, J.; Prater, C. B.; Hansma, P. K. *Phys. Rev. B* **1990**, *42*, 9255. (f) Dai, Z.; Slough, C. G.; Coleman, R. V. *Phys. Rev. Lett.* **1991**, *66*, 1318. (g) Burk, B.; Thomson, R. E.; Zettl, A.; Clarke, J. *Phys. Rev. Lett.* **1991**, *66*, 1991. (h) Wang, C.; Slough, C. G.; Coleman, R. V. J. *Vac. Sci. Technol. B* **1991**, *9*, 1044. (j) Raina, G.; Sattler, K.; Muller, U.; Vekateswaran, N.; Xhie, J. J. *Vac. Sci. Technol. B* **1991**, *9*, 1027. (m) Enomoto, H.; Ozaki, H.; Suzuki, M.; Fujii, T.; M. Yamaguchi *J. Vac. Sci. Technol. B* **1991**, *9*, 1022. (n) Giambattista, B.; Slough, C. G.; McNairy, W. W.; Coleman, R. V. *Phys. Rev. B* **1990**, *41*, 10082.

(9) (a) Wu, X. L.; Lieber, C. M.; Ginly, D. S.; Baughman, R. J. *Appl. Phys. Lett.* **1989**, *55*, 2129. (b) Parks, D. C.; Wang, J.; Clark, N. A.; Hermann, A. M. *Appl. Phys. Lett.* **1991**, *59*, 1506. (c) Coleman, R. V.; Drake, B.; Hansma, P. K.; Slough, G. *Phys. Rev. Lett.* **1985**, *55*, 394.

(10) (a) Bai, C.; Dai, C.; Zhu, C.; Chen, Z.; Huang, G.; Wu, X.; Zhu, D.; Baldeschwieler, J. D. *J. Vac. Sci. Technol. A* **1990**, *8*, 484. (b) Yoshimura, M.; Shigekawa, H.; Nejoh, H.; Saito, G.; Saito, Y.; Kawazu, A. *Phys. Rev. B* **1991**, *43*, 13590. (c) Bando, H.; Kashiwaya, S.; Tokumoto, H.; Anzai, H.; Kinoshita, N.; Kajimura, H. *J. Vac. Sci. Technol.* **1990**, *A8*, 479. (d) Yoshimura, M.; Ara, N.; Kageshima, M.; Shiota, R.; Kawazu, A.; Shigekawa, H.; Saito, Y.; Oshima, M.; Mori, H.; Yamochi, H.; Saito, G. *Surf. Sci.* **1991**, *242*, 18.

(11) (a) Fainchtein, R.; Murphy, J. C. *J. Vac. Sci. Technol. B* **1991**, *9*, 1013. (b) Pan, S.; Delozanne, A. L.; Fainchtein, R. *J. Vac. Sci. Technol. B* **1991**, *9*, 1017. (c) Li, S.; White, H. S.; Ward, M. D. *J. Phys. Chem.* **1992**, *96*, 9014.

(12) Sleator, T.; Tycko, R. *Phys. Rev. Lett.* **1988**, *60*, 1418.

(13) (a) Li, S.; White, H. S.; Ward, M. D. *Chem. Mater.* **1992**, *4*, 1082. (b) Magonov, S. N.; Schuchardt, J.; Kempf, S.; Keller, E.; Cantow, H.-J. *Synth. Met.* **1991**, *40*, 59. (c) Magonov, S. N.; Kempf, S.; Rotter, H.; Cantow, H.-J. *Synth. Met.* **1991**, *40*, 73.

(14) Morssink, H.; van Bodegom, B. *Acta Crystallogr.* **1980**, *B37*, 107.

(15) Strzelecka, H.; Veber, M.; Zinsou, A.-T.; Bassoul, P.; Petit, P.; Bieber, A.; André, J.-J. *J. Mater. Chem.* **1993**, *3*, 59.

Table 1. Lattice Constants and Densities for TCNQ-Layered Materials as Determined from X-ray Diffraction and STM[a]

material	space group	X-ray (Å)	STM (Å)	density (g/cm³)
(DEM) $(TCNQ)_2$ (**1a**)[14]	$P\bar{1}$	a = 7.902(4)	a = 8.0 ± 0.3	1.255
		b = 28.134(6)	(b)	
		c = 7.514(3)	c = 7.8 ± 0.3	
		α = 91.26(6)°	(b)	
		β = 118.47(4)°	β = 120 ± 0.2°	
		γ = 93.67(2)°	(b)	
(MEM)$(TCNQ)_2$ (**1b**)[21]	$P1$	a = 7.824(5)	a = 6.9 ± 0.3	1.261
		b = 15.426(16)	(b)	
		c = 6.896(5)	c = 5.7 ± 0.3	
		α = 113.59(8)°	(b)	
		β = 73.27(7)°	β = 78 ● 2°	
		γ = 112.71(8)°	(b)	
DMM$(TCNQ)_2$ (**1c**)[23] (monoclinic)	$P2_1/m$	a = 7.52(2)[c]	a = 7.2 ± 0.3	1.289
		b = 26.814(8)	(b)	
		c = 7.594(7)	c = 7.5 ● 0.3	
		β = 58.44(6)°	β = 56 ± 2°	
DMM$(TCNQ)_2$ (**1d**)[24] (triclinic)	$P\bar{1}$	a = 16.452(3)	(b)	1.352
		b = 12.838(3)	b = 11.4 ± 0.3	
		c = 6.592(2)	c = 6.0 ± 0.3	
		α = 103.18(2)°	α = 98 ± 2°	
		β = 98.79(2)°	(b)	
		γ = 103.25(2)°	(b)	
(VIN)$(TCNQ)_2$ (**2**)[15]	$P\bar{1}$	a = 7.483(3)	a = 7.3 ± 0.3	1.302
		b = 7.792(1)	b = 8.1 ± 0.3	
		c = 30.547(4)	(b)	
		α = 7.483(3)°	(b)	
		β = 92.85(2)°	(b)	
		γ = 113.98(3)°	γ = 115.0 ± 2°	

[a] Uncertainty in lattice constants determined by STM represents 2σ. [b] Could not be measured since corresponding face could not be measured. [c] Based on indexing of crystal and is 0.27 Å smaller than reported X-ray value.

periodicity of the *local* density of states (LDOS) will correspond to the orientation and spatial extension of the molecular orbitals localized on the molecules exposed at the crystal plane under examination. This is particularly appropriate for crystalline molecular semiconductors, for which the electronic structure can be described by a tight-binding approximation, which invokes substantial localization of electronic states on molecular sites.[16] Therefore, in the following section, the STM data will be described along with the molecular structure of the appropriate crystal plane. Table 1 summarizes the crystallographic parameters of the charge-transfer salts and the corresponding lattice constants determined from the STM data.

(*N*,*N*′-Diethylmorpholinium)$^+$(TCNQ)$_2^-$ (1a). The crystal structure of the crystalline conductor (*N*,*N*′-diethylmorpholinium)$^+$(TCNQ)$_2^-$ (**1a**) reveals *two crystallographically inequivalent ac* layers of TCNQ molecules, which are separated by *N*,*N*′-diethylmorpholinium$^+$(DEM$^+$) cation layers (Figure 1).[14] The layering motif can be described as ...·DEM$^+$·A·DEM$^+$·B·... along the *b* direction, where A and B represent the crystallographically inequivalent TCNQ layers. The topography of these layers can be visualized from space-filling models

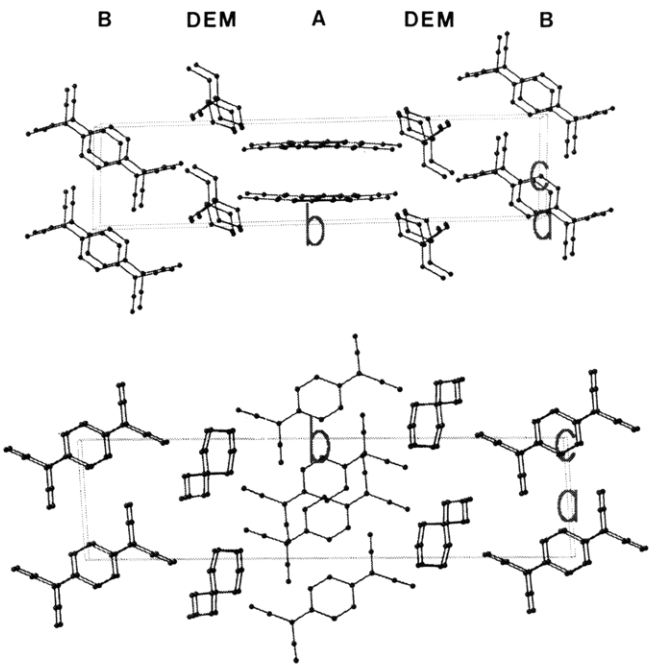

Figure 1. Unit cell of **1a** viewed along the *a* (top) and *c* (bottom) axes. The *ac* planes contain TCNQ anion and DEM$^+$ cation stacks, which are identified at the top of the figure. Hydrogen atoms have been omitted for clarity.

based on the crystal structure (Figure 2). The TCNQ layers contain $(TCNQ)_2^-$ dimers (i.e., the charge per molecule is ρ = 0.5–). The TCNQ molecules constituting the dimers in layer A exhibit the common shifted ring-over-ring motif (molecules A and A′ in Figure 2), with a rather large separation between planes in the dimers (3.41 Å). The interdimer overlap motif, however, does not provide significant overlap of the TCNQ molecules (molecules A′ and A″), although the interdimer spacing is rather small (3.19 Å). In contrast, layer B has $(TCNQ)_2^-$ dimers with a ring-external bond overlap motif, stacked along the *c* axis. The intradimer spacing is 3.14(1) Å (molecules B and B′), and the interdimer spacing is 3.36(1) Å (molecules B′ and B″). Inspection of the structure of these layers reveals that the planes of the $(TCNQ)_2^-$ dimers in layers A and B are subtend angles of 0° and 60° with the *a* axis, respectively. Furthermore, layer A forms a two-dimensional network with significant interdigitation of the TCNQ stacks, while layer B is better described as an assembly of discrete one-dimensional TCNQ stacks. Layer B also exhibits a greater degree of surface corrugation along the [10$\bar{1}$] direction, parallel to the molecular TCNQ plane, than does layer A along the [100] direction, also parallel to the molecular TCNQ plane.

Upon crystallization, **1a** forms large *ac* faces with large, molecularly flat terraces and relatively few defects, as revealed by large scale (700 nm × 700 nm) STM images (Figure 3). The tunneling current contrast between the terraces is consistent with vertical steps of approximately 8 and 20 Å, roughly equal to the heights of one and two DEM$^+$TCNQ$^-$ layers, respectively. The presence of these large terraces is consistent with the observed bulk morphology and slow growth normal to the *ac* face.

Molecular scale images of the *ac* face of **1a** reveal a $\rho(r,E_F)$ that consists of rectangular-shaped LDOS (Figure 4) oriented along different directions, these directions subtending an angle of 120 ± 1°, nearly identical to the value of β (118.47°). The average periodicity of the LDOS along

(16) (a) Slater, J. C.; Koster, G. F. *Phys. Rev.* **1954**, *94*, 1498. (b) Bloch, F. *Z. Phys.* **1928**, *52*, 555. (c) Epstein, A. J.; Miller, J. S. *Prog. Inorg. Chem.* **1976**, *20*, 1. (d) Garito, A. F.; Heeger, A. J. *Acc. Chem. Res.* **1974**, *7*, 232–240.

(17) Parks, D. C.; Wang, J.; Clark, N. A.; Hermann, A. M. *Appl. Phys. Lett.* **1991**, *59*, 1506.

(18) Parkinson, B. *J. Am. Chem. Soc.* **1990**, *112*, 7498.

(19) (a) Kobayashi, A.; Grey, F.; Williams, R. S.; Aono, M. *Science* **1993**, *259*, 1724. (b) Stroscio, J. A.; Eigler, D. M. *Science* **1991**, *254*, 1319. (c) Becker, R. S.; et al. *Nature* **1987**, *325*, 419. (d) Lyo, I.-W.; Guethner, P. H.; Rugar, D. *Phys. Rev. Lett.* **1990**, *65*, 2418.

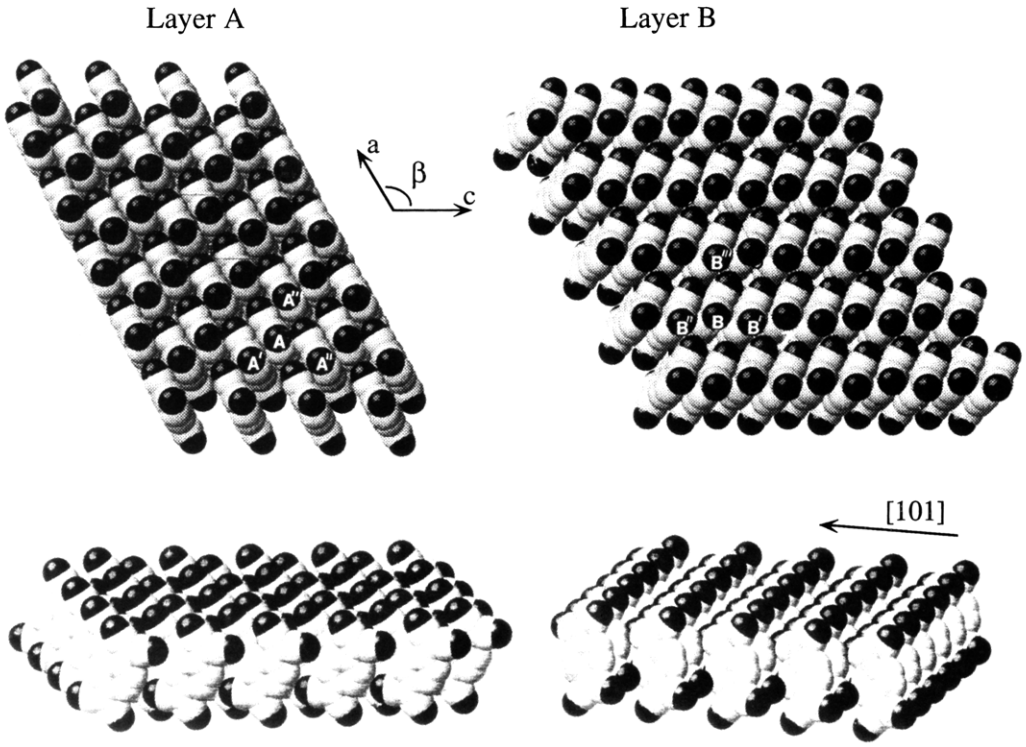

Figure 2. Space-filling models of the crystallographically inequivalent TCNQ layers A and B in **1a** viewed normal to the layers (top) and nearly parallel to the layers (bottom). It is evident from these models that layer A has a two-dimensional motif with only a slight corrugation along the [100] direction, whereas layer B is better described as one-dimensional with significant corrugation along the [101] direction. The planes of the TCNQ molecules in layer A are oriented parallel to the *a* axis, whereas the planes of the TCNQ molecules in layer B are oriented 60° with respect to the *a* axis. Molecules A–A′ and B–B′ represent the constituents of the $(TCNQ)_2^-$ dimer in each stack, whereas A–A″ and B–B″ represent the interdimer molecular contacts. Molecules A‴ and B‴ are crystallographically identical to A″ and B″, respectively. This notation is identical to that used in ref 14.

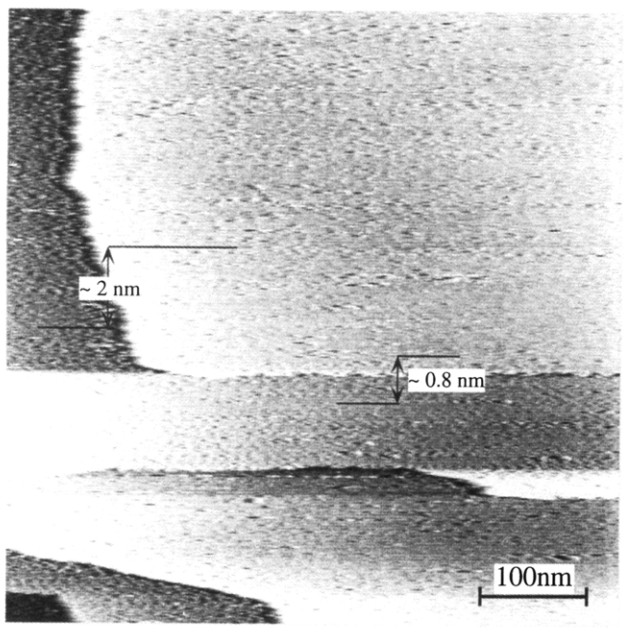

Figure 3. Large area STM scan of the *ac* surface of **1a**. The presence of large molecularly flat regions with relatively few defect regions suggests an energetically stable surface structure of the organic TCNQ molecules. The presence of large terraces is indicative of a relatively large growth rate along the stacking direction of the TCNQ molecules with a smaller growth rate perpendicular to the *ac* plane.

one of these directions is 7.8 ± 0.2 Å, in reasonable agreement with the value of *c* obtained from the crystal structure (*c* = 7.514 Å). The average periodicity of the LDOS along the other direction is 8.0 ± 0.2 Å, in good agreement with the *a* lattice parameter (7.902 Å). The tunneling current contrast therefore is consistent with the structure of the *ac* plane. This plane may be terminated with either $TCNQ^{0.5-}$ or DEM^+ molecules, as required for electroneutrality. The observation that the lattice parameters obtained with STM agree with those expected for the *ac* plane argues against surface reconstruction, in agreement with the other STM investigations of molecular crystals.[13–15] Occasional defects observed in these images appear to correspond to missing molecules. While these defects perturb the immediately surrounding tunneling current features, the effect on next-nearest LDOS is negligible.

The STM images in Figures 3 and 4 were captured at a setpoint current less than 0.1 nA. Setpoint currents exceeding 1 nA, however, resulted in images whose appearance changed in successive scans. This behavior suggested that etching of the *ac* face was occurring during data acquisition under these conditions. Previous reports have demonstrated STM-induced etching of other two-dimensional layered materials under suitable conditions.[17–19] While etching processes induced by STM are not well understood, etching of **1a** occurs when the bias voltages and/or setpoint currents exceed a critical value. Etching may occur by one of several mechanisms, including field-induced ionization of the surface molecules, thermal ionization, field-assisted evaporation, or direct tip–sample contact. All of these mechanisms are consistent with the observation that etching of **1a** occurs at higher tunneling currents, but no further attempt has been made to identify the mechanism responsible for the etching behavior seen here.

The etching of **1a** can be halted by reduction of the setpoint current to its original value, upon which stable

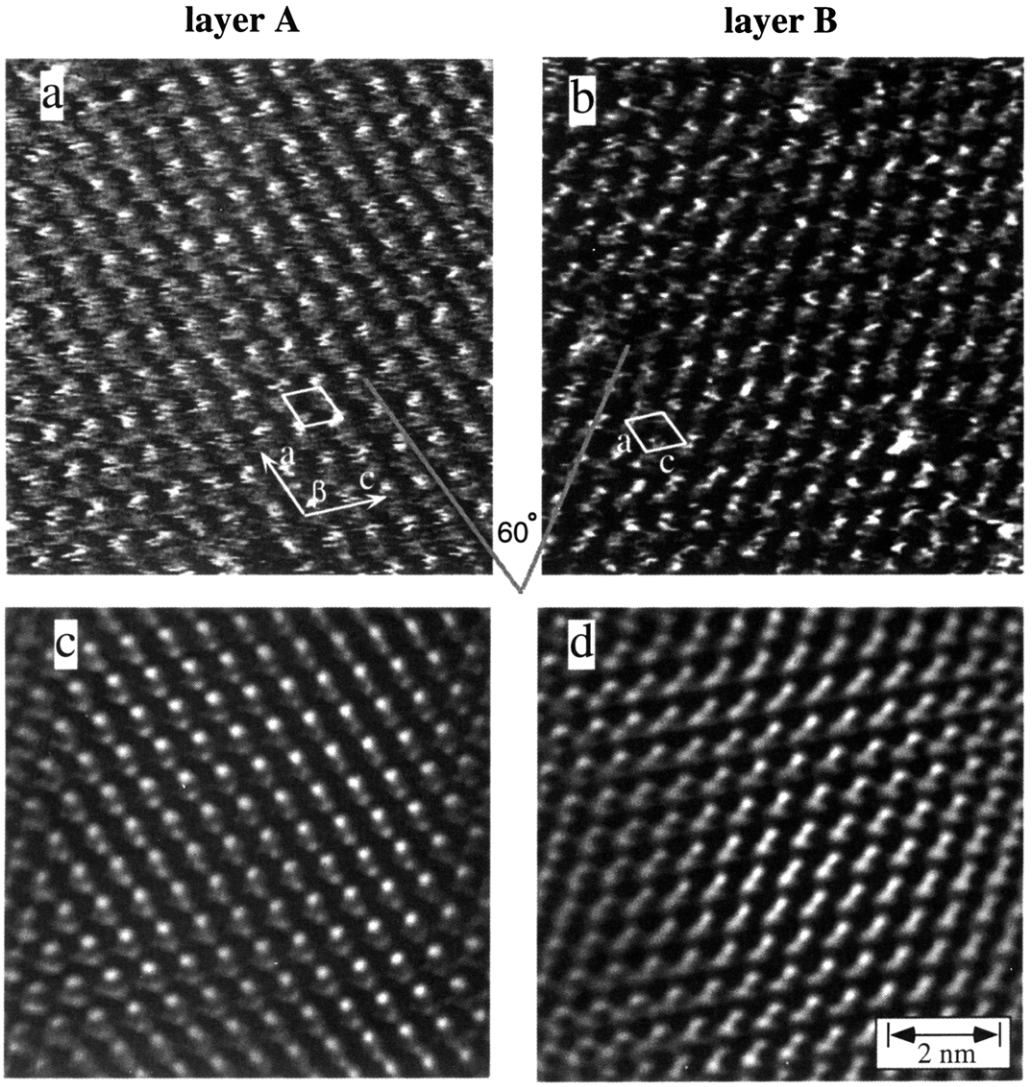

Figure 4. (a, b) Raw STM data of the *ac* face of **1a**, depicting the LDOS of the two crystallographically inequivalent TCNQ layers (A and B), in which the image on the right side was acquired after etching at higher tunneling currents. The tunneling current features repeat at intervals of *a* and therefore can be assigned to $(TCNQ)_2^-$ dimers, which repeat at *a* in the crystal structure. The image on the left is assigned to layer A because the LDOS assigned to the $(TCNQ)_2^-$ dimers are parallel to the *a* axis and have a two-dimensional motif, in agreement with the crystal structure of layer A. The LDOS in the image on the right side are oriented at an angle of 60° with respect to the *a* axis and are better described as one-dimensional, consistent with the structural motif of layer B. (c, d) Fourier filtered images corresponding to the raw data in (a, b). Filtering was performed by selecting first-order frequencies having the highest density amplitude, using the commercially available software provided by Digital Instruments with the Nanoscope II scanning tunneling microscope. Tunneling conditions: tip bias = −1815.8 mV, setpoint current = 0.10 nA. Maximum contrast of tunneling current corresponds to 1.1 Å in (a) and (b). The values of *a*, *c*, and β are in reasonable agreement with the X-ray crystal structure (see Table 1).

images of regions with low defect density can once again be obtained. Figure 4b depicts an image acquired at the lower tunneling current after etching in which the LDOS differ from the original image. In the case of Figure 4a, the long axes of these features are oriented parallel to the *a* axis, *identical to the orientation of the* $(TCNQ)_2^-$ *dimers in layer A*. In contrast, the long axes of the LDOS after a typical etching sequence (Figure 4b) were oriented 60° with respect to the *a* axis, *identical to the orientation of the* $(TCNQ)_2^-$ *dimers in layer B*. These observations are consistent with assignment of the STM data in Figure 4 to independent TCNQ layers A and B. In both images there is substantial corrugation of the LDOS along the *c* axis, which can be attributed to the highly localized dimer structure in both layers. The dimer structure associated with the $4k_F$ state of **1a** is consistent with appreciable state density between molecules in the $(TCNQ)_2^-$ dimer, with the excess electron delocalized over the dimer.[20] The electronic structure of the one-dimensional $4k_F$ state predicts that the tunneling current contrast will depend upon the nature of the electronic states near the top of the valence band (for positive tip biases) or near the bottom of the conduction band (for negative tip biases). According to a tight binding band approximation, these states have nodes between $(TCNQ)_2^-$ dimers at intervals of *c*, consistent with the observed corrugation of $\rho(r,E_F)$ along *c*.[13a] In both layers the diminished state density between $(TCNQ)_2^-$ dimers would result in decreased tunneling current between the dimers. It is important to note that attempts to image simultaneously two adjacent regions exhibiting the layer A and B LDOS were not successful, as the steps separating these regions were not stable when imaging at high resolution.

The TCNQ dimers in layer A are interdigitated, resulting in a two-dimensional motif. This is consistent with the data in Figure 4a, which display a more continuous

tunneling current along a than the data in Figure 4b assigned to layer B, which consists of discrete one-dimensional TCNQ stacks. The minimal corrugation of $\rho(r,E_F)$ along the a axis in Figure 4a also agrees qualitatively with the molecular topography of layer A along the a axis, whereas the LDOS in the interstack regions of layer B is expected to be less than that of layer A, in qualitative agreement with the data in Figure 4b. Layer B also is more highly corrugated along the [101] direction, parallel to the TCNQ planes, than is layer A along the analogous [100] direction. This results in a greater variation in distance between individual methylidene carbon atoms of the TCNQ dimers and the scanning STM tip along the [101] direction in layer B, in agreement with the STM data. Therefore, the STM images of both layers exhibit LDOS periodicity along the c axis that is expected for the $4k_F$ state, but the subtle differences in tunneling current contrast reflects differences in the dimensionalities of the two layers. Interestingly, EPR studies of **1a** indicated that the TCNQ stacks in layer B undergo a spin-Peierls transition at 23 K. However, layer A was stable to a phase transition at temperatures <1.5 K. This stability has been attributed to the higher dimensionality of layer A. Two $S = {}^1/_2$ resonances were assigned to each of the inequivalent TCNQ layers, with the $g(\theta)$ dependence corresponding to the 60° dihedral angle between the TCNQ stacking directions in the two layers. The STM data described herein corroborate the assignment of the $4k_F$ electronic structure and reveal the differences between the dimensionalities of the electronic subsystems of layers A and B.

(Vinamidinium)$^+$(TCNQ)$_2^-$ (2). The crystal structure of **2** reveals two crystallographically inequivalent TCNQ stacks assembled into two crystallographically inequivalent TCNQ layers separated by VIN^+ cation layers, to give a motif ...·VIN^+·A·VIN^+·B·... motif (Figure 5a).[15] The TCNQ layers differ with respect to their structural dimensionalities, and presumably their electronic properties. Upon crystallization, **2** forms large ab faces that are amenable to STM examination. STM data collected at high resolution reveal LDOS whose periodicity is in good agreement with the ab lattice parameters determined from the X-ray single-crystal structure (Figure 5b). This suggests negligible surface reconstruction, similar to the behavior observed for **1a**. However, the quality of the images obtained for **2** was never as satisfactory as those of **1a**, and repeated attempts to detect both crystallographically inequivalent TCNQ layers were not successful. Notably, EPR measurements suggest a relatively large disparity in the ionicity ($\rho_{TCNQ_A} = {}^2/_3-$ and $\rho_{TCNQ_B} = {}^1/_3-$) of the TCNQ layers, presumably because of hydrogen bonding of TCNQ layer A with neighboring vinamidinium cation layers that is less prevalent in layer B. This hydrogen bonding may favor layer A over layer B at the surface. The A layer has been reported to exhibit narrow-gap semiconducting behavior in which there is a strong decrease in the density of states at the Fermi level. This may be the source of the difficulty in obtaining higher quality images of the ab face.

(*N*-Methyl-*N*'-ethylmorpholinium)$^+$(TCNQ)$_2^-$ (1b). The crystal structure of **1b** reveals the presence of $(TCNQ)_2^-$ dimers stacked along the c axis (Figure 6a).[21] These stacks are assembled into equivalent ac layers

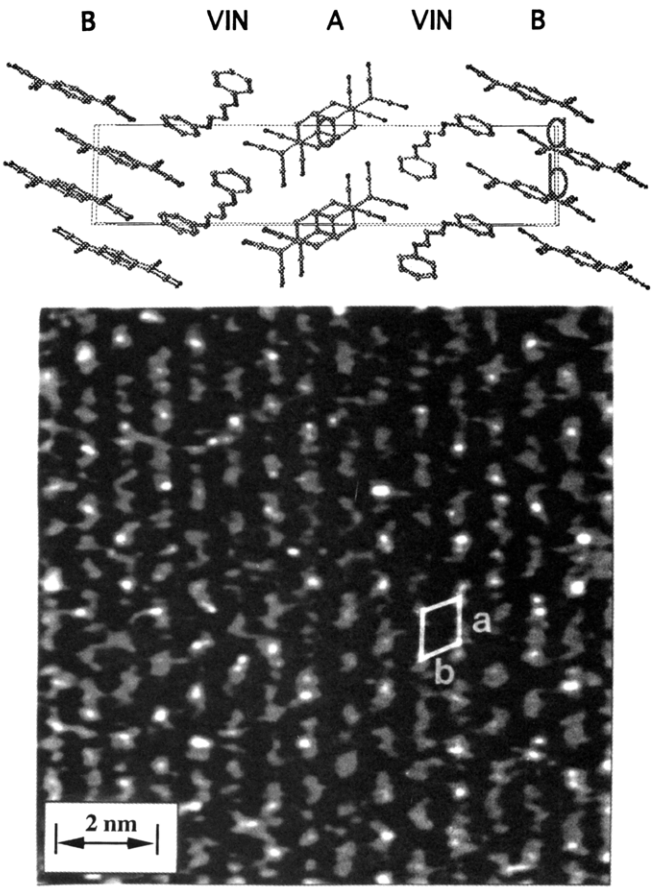

Figure 5. Top: unit cell of **2** showing the orientation and stacking direction of the crystallographically inequivalent A and B TCNQ columns. Bottom: STM image of the ab face of **2** showing the pattern of LDOS. Although there is agreement of the STM lattice parameters with the X-ray values (Table 1), the difficulty in acquiring high-quality **2** molecular scale images has rendered assignment of this layer impossible. Tunneling conditions: setpoint current = 0.21 nA, tip bias = −266.4 mV.

separated by MEM^+ cations to give ...·MEM^+·A^-·MEM^+·A^-·... motif. The TCNQ molecules exhibit a one-dimensional motif with significant molecular corrugation in the ac plane along both the c and a directions (Figure 6b), reminiscent of the structure of the B layer of **1a**. Crystals of **1b** exhibit large ac faces which are amenable to STM investigation. The general pattern of the LDOS observed in the STM data of **1b** resembles that expected based on the structure of the ac plane (Figure 6c). However, the LDOS periodicity is nearly 15% shorter than the corresponding lattice parameters determined from the X-ray crystal structure data. This discrepancy is significantly larger than the error typically encountered in room temperature STM studies, suggesting some reconstruction and compression of the surface ac layer.

Notably, larger scale corrugations with periodicities of 75–100 Å superimposed on the molecularly resolved DOS are also observed. This resembles behavior reported previously for graphite,[22] in which large scale corrugations were attributed to elastic deformation of the surface as a result of deformation by direct tip–sample interactions or contamination-mediated deformation of the sample by the STM tip. These effects would be most significant for samples with a small elastic modulus in the direction

(20) Bechgaard, K. *Structure and Properties of Molecular Crystals*; Pierrot, M., Ed. Elsevier: New York, 1990; p 194.
(21) Bosch, B.; van Bodegom, B. *Acta Crystallogr.* **1977**, *B33*, 3013.
(22) (a) Mamin, H. J.; Ganz, E.; Abraham, D. W.; Thomson, R. E.; Clarke, J. *Phys. Rev. B* **1986**, *34*, 9015. (b) Soler, J. M.; Baro, A. M.; Garcia, N.; Rohrer, H. *Phys. Rev. Lett.* **1986**, *57*, 444.

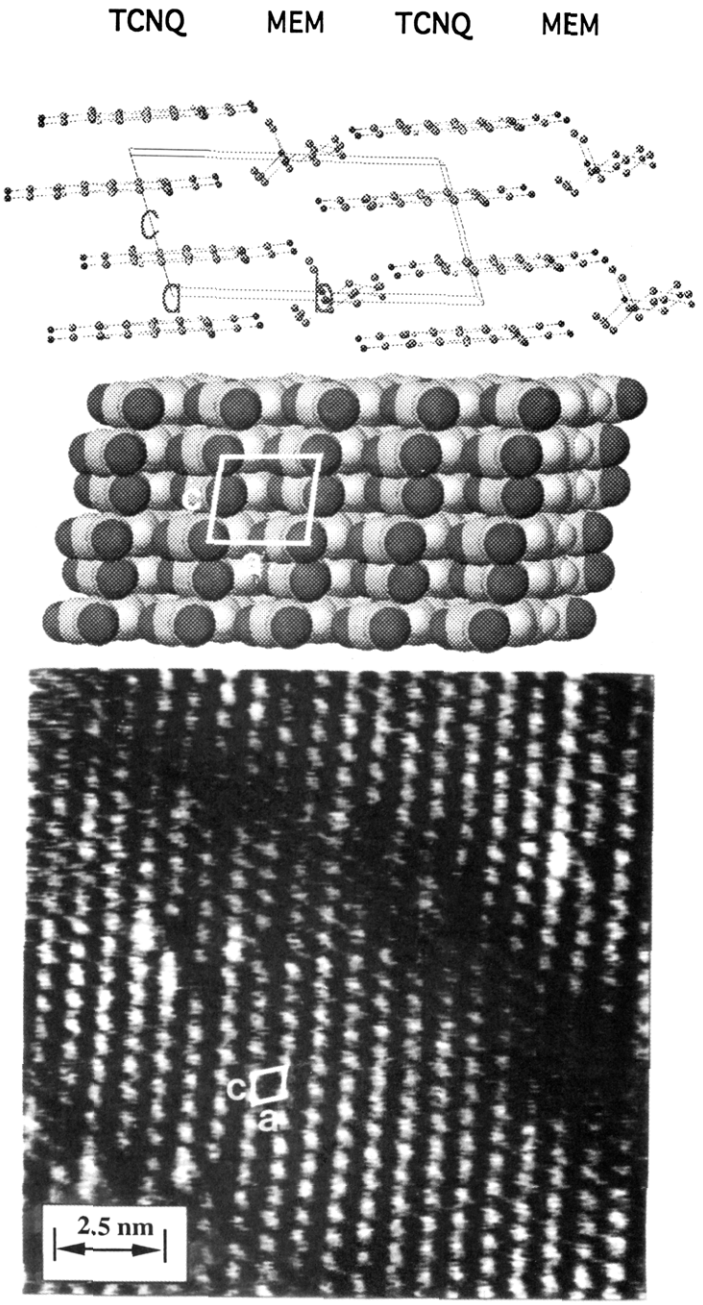

Figure 6. Top: Unit cell of the **1b**. Middle: Space-filling model of the *ab* surface of the MEM $(TCNQ)_2$ crystal surface. The corrugation along *c* is a manifestation of the ring-external bond overlap of the individual TCNQ dimers, while the pronounced *one-dimensional stacking of the dimers along c produces a* relatively large corrugation along *a*. Bottom: STM image of the *ac* face of **1b** showing the LDOS arising from the position of the $(TCNQ)_2^-$ dimers. Large-scale corrugation and point defects (i.e., missing molecules) are common observations in the homologous systems presented here. Tunneling conditions: setpoint current = 0.59 nA, tip bias = −271.0 mV.

normal to the surface, as expected for these layered TCNQ charge-transfer salts. The observation of the large scale corrugations are consistent with the lattice compression evident from the LDOS periodicity: the weak interactions between *ac* layers that allow facile tip-induced deformation of the layers would not inhibit the reconstruction of the surface *ac* layer to a denser plane with a lower free energy.

(*N*,*N*′-Dimethylmorpholinium)$^+$(TCNQ)$_2^-$ (Monoclinic, 1c; Triclinic, 1d). The dimorphic phase behavior of (*N*,*N*′-dimethylmorpholinium)$^+$$(TCNQ)_2^-$ provides an excellent opportunity to examine the relationship between

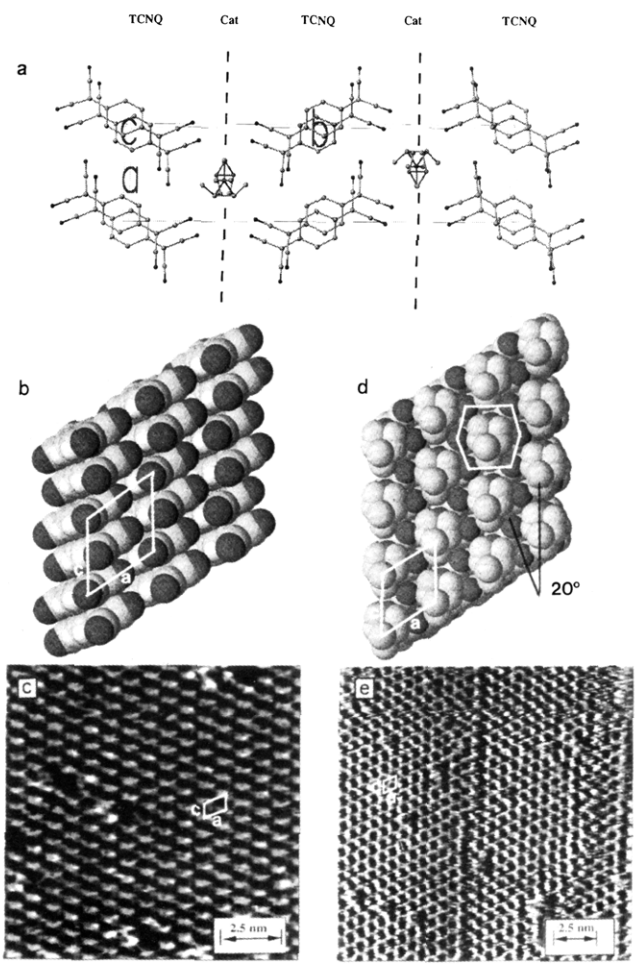

Figure 7. (a) Unit cell of monoclinic **1c**. The TCNQ molecules form dimer pairs which stack along the *c* axis and which form layers parallel to the *ac* crystalline plane. Each of the layers are crystallographically equivalent and are related to one another by a mirror plane. (b) Space-filling model of the *ac* surface of the monoclinic DMM $(TCNQ)_2$ polymorph. The packing of the individual TCNQ dimers result in the formation of an hexagonal network on the *ac* surface. (c) STM image of the *ac* surface which clearly demonstrates the hexagonal LDOS arising from the $(TCNQ)_2^-$ dimers. (d) Space-filling model of the *ac* surface of **1c** covered with DMM^+ cations. The packing of the cations results in a partially covered TCNQ surface displaying a honeycomb network visible through the cation layers. (e) STM image of the *ac* surface revealing the honeycomb network of LDOS arising from the cations obscuring the $(TCNQ)_2^-$ dimers. Tunneling conditions for both images: setpoint current = 0.54 nA, tip bias = −1145.0 mV. Maximum contrast of tunneling current corresponds to 12.0 Å.

STM tunneling characteristics and subtle differences in the molecular structure of crystal planes of salts with identical stoichiometric composition. The structure of *monoclinic* $P2_1/c$ **1c** *reveals stacks of* $(TCNQ)_2^-$ dimers oriented along the *c* axis, with the shifted ring–ring overlap.[23] The stacks are arranged into crystallographically equivalent *ac* layers, which are related to each other by a mirror plane, these layers separated by layers of disordered DMM^+ cations (Figure 7a) to give a ...·DMM^+·A^-·DMM^+·A^-·... motif. The molecular motif of the TCNQ layers, with interdigitated $(TCNQ)_2^-$ dimers, is reminiscent of layer A in **1a**. In contrast, triclinic $P\bar{1}$ **1d** possesses $(TCNQ)_2^-$ dimers assembled into discrete one-dimensional stacks along the *c* axis, with the TCNQ molecules in each dimer related by a ring-over-external

(23) Kaminga, P.; van Bodegom, B. *Acta Crystallogr.* **1980**, *B37*, 114.

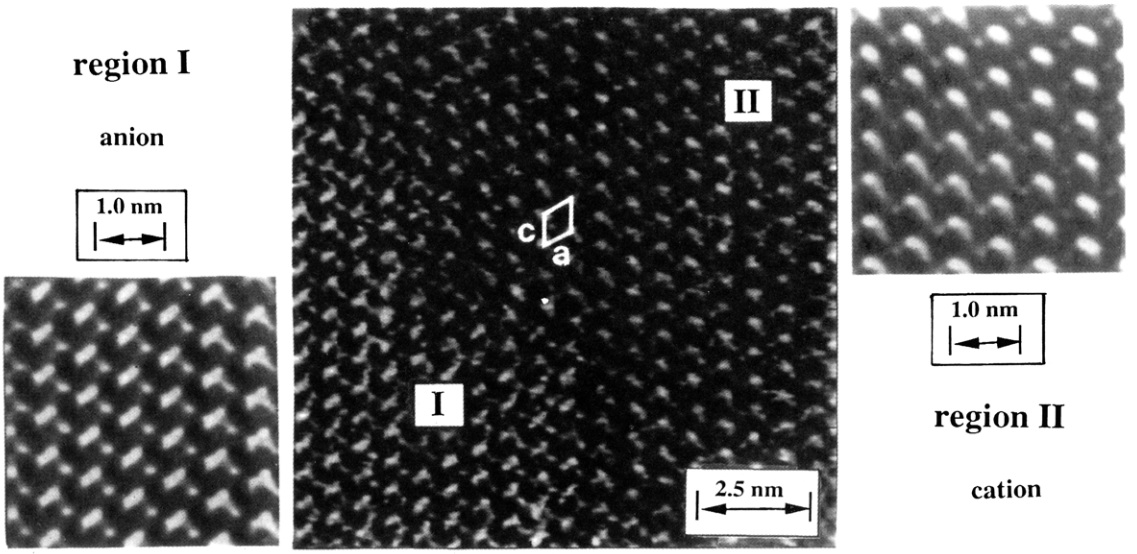

Figure 8. Large-area scan of the *ac* surface of **1c** recorded under lower tunneling bias than the data in Figure 7. Two regions (I and II) are observed. The different LDOS in the two regions may be attributed to differences in the identity of the ions (i.e., either cations or anions) terminating the surface. A height profile across both regions indicates no difference in heights. Tunneling conditions: setpoint current = 0.54 nA, tip bias = −1067.5 mV. Maximum contrast of tunneling current corresponds to 9.0 Å. The images in the smaller panels are Fourier filtered representations of the two different regions. Filtering was performed by selecting first-order frequencies having the highest density amplitude, using the commercially available software provided by Digital Instruments with the Nanoscope II scanning tunneling microscope.

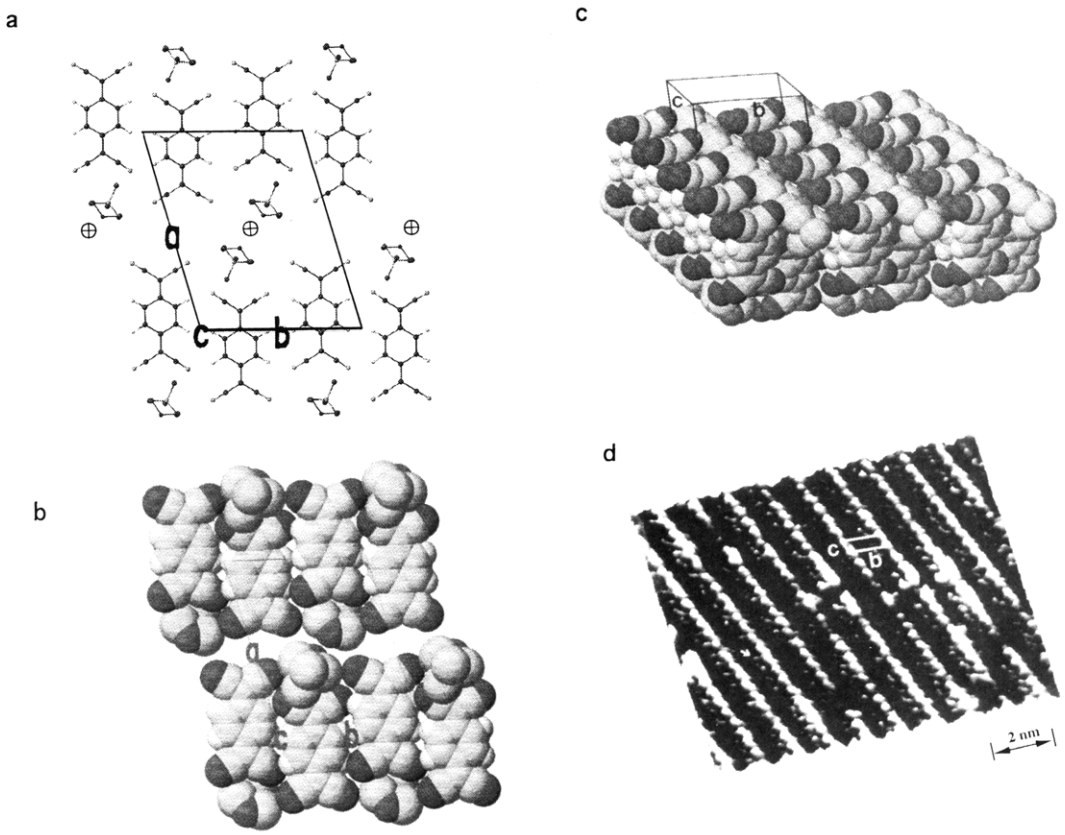

Figure 9. (a, b) Unit cell of the triclinic **1d** as viewed down the *c* stacking axis. (c) View of the *bc* surface layer. Note also the asymmetrical placement of the DMM^+ cations (hydrogens omitted for clarity) between TCNQ stacks in which the methyl groups of the DMM^+ cation lie to one side of the cation channel. (d) STM image of the *bc* surface depicting the LDOS stemming from the $(TCNQ)_2^-$ dimers along the *c* stacking axis. Minor tunneling features (indicated by the arrow) appearing to the left of the major features assigned to the TCNQ stacks are attributed to the asymmetric field provided by an enantiotopic set of DMM^+ cations. Tunneling conditions: setpoint current = 0.21 nA; tip bias = −1759.0 mV.

bond overlap (Figure 9a).[24] This results in significant molecular corrugation along the *c* axis. The most notable structural feature of the *bc* plane is the hill-and-valley structure traversing the *b* direction in which the TCNQ stacks (hills) and DMM^+ cations (valleys) repeat with a periodicity of *b* (Figure 9b). It is important to note that an inversion center lies between DMM^+ cations of adjacent

(24) (e) Steurer, W.; Visser, R. J. J.; van Smaalen, S.; De Boer, J. L. *Acta Crystallogr.* **1987**, *B43*, 567.

bc layers. Consequently, the DMM^+ cations in a surface *bc* layer belong to an enantiotopic set comprising one-half of the inversion related pairs.

STM Images of 1c. Crystals of **1c** exhibit large *ac* faces which are amenable to STM investigation. Large-scale STM images of the *ac* face of **1c** typically display large, molecularly flat regions separated by steps of approximately 22 Å, nearly equivalent to the *b* lattice parameter of **1c**. Images acquired at higher resolution reveal LDOS with a periodicity and orientation in good agreement with the X-ray lattice parameters of the *ac* plane (Figure 7c). The LDOS features clearly repeat along the *c* axis at intervals of *c*, identical to the repetition of the symmetry equivalent $(TCNQ)_2^-$ dimers. Defects are evident that appear to correspond to missing $(TCNQ)_2^-$ dimers. Interestingly, under identical tunneling conditions, other regions of the same crystal face display a hexagonal network of LDOS resembling a honeycomb motif (Figure 7e). The LDOS periodicity in these regions also is identical to the X-ray structure lattice parameters of the *ac* plane. The observation of two different STM images on the same crystal face is strong evidence that one of these images represents an *ac* face terminated with TCNQ anions, whereas the other represents an *ac* face terminated with DMM^+ cations. On the basis of comparisons with molecular models of the *ac* plane and the lack of density of states at the Fermi level on the DMM^+ cations, is reasonable to assign the honeycomb motif in Figure 7e to cation terminated regions (Figure 7d). The cations on the *ac* surface layer obscure much of the underlying TCNQ molecules, and a hexagonal array of TCNQ nitrogen atoms exposed in the regions not covered by the cations is clearly evident from the model. While the mediating effect of the cations on the tunneling current is difficult to predict, the hexagonal molecular array is consistent with the orientation and periodicity of the LDOS observed in the STM images of these regions. Both the anion and cation covered regions are stable indefinitely to scanning under the conditions employed.

It is interesting to note that the STM images of the *ac* face of **1c** are highly sensitive to tunneling conditions. Smaller bias voltages and setpoint currents afforded images with generally poorer tunneling current contrast than the images described in the preceding paragraph. However, these conditions allowed imaging, in the same frame, of regions displaying LDOS that were dramatically different with respect to their orientation (labeled I and II in Figure 8). These boundaries between these regions were unstable to imaging at higher tunneling bias and tunneling conditions. A height profile analysis across regions I and II in Figure 8 revealed no appreciable difference in heights of the two regions. Since the mirror plane is parallel to the surface, it is unlikely that these regions result from twinning. It is therefore reasonable to suggest that this image contains regions terminated in TCNQ anions *and* DMM^+ cations. However, in contrast to the data in Figure 7, the assignment of the LDOS observed under these tunneling conditions to either anion or cation terminated regions is less clear. Rather, the different LDOS orientations may be due to the poorly understood mediation of the tunneling current by the cations at these lower tunneling biases and current. It is interesting to note the presence of minor tunneling features oriented along the $[\bar{1}01]$ direction, which are not evident in Figure 7. These features are suggestive of interstack electronic interaction between TCNQ anions, which are in close proximity along $[\bar{1}01]$. Close interstack contacts are *not* present along [101], consistent with the absence of tunneling features along this direction.

STM Images of 1d. Crystals of **1d** exhibit large *bc* faces which are amenable to STM investigation. The tunneling current contrast of the *bc* face of **1d**, differs substantially from that of the *ac* face of **1c**, even though both planes can be described as TCNQ molecular layers. In the case of **1d**, clearly distinct hill-and-valley structure is observed in the STM tunneling current (Figure 9d). The periodicity of the LDOS is in good agreement with the X-ray structure lattice parameters of the *bc* plane, although the slightly smaller STM values (ca. 10% smaller) suggest compression of the surface layer. The corrugation of $\rho(r,E_F)$ along the *c* axis reflects the slipped ring-external bond arrangement of TCNQ anions in the dimers, as this arrangement results in topographic corrugation along the *c* axis. The more extensive corrugation along the *b* axis, however, reflects the hill-and-valley structure of the TCNQ stacks within this plane. The hills observed in the tunneling current can be assigned to the TCNQ stacks exposed at the surface plane. The significantly smaller tunneling current in the valleys can be attributed to adjacent TCNQ stacks recessed from the surface and obscured from the STM tip by the DMM^+ cations, which do not possess a significant DOS at the Fermi level.

Close examination of the STM data reveals a set of minor tunneling features repeating with the lattice periodicity of the *bc* plane *on the left side* of the major tunneling features which were assigned above to the TCNQ molecules closest to the STM tip. These features are consistent with the structure of the *bc* plane, which is enantiotopic under the $P\bar{1}$ symmetry as a result of the inversion center located between the *bc* planes. In a given *bc* plane, all the DMM^+ cations belong to a single enantiotopic set in which the cations are oriented asymmetrically on the *bc* plane (in the $P\bar{1}$ space group there is no mirror plane or inversion center relating the molecules within the *bc* plane). The asymmetry of the minor tunneling feature, therefore, can be attributed to the mediation of the tunneling current by the asymmetric field of a single enantiotopic set of cations.

The electronic and magnetic properties of both dimorphs **1c** and **1d** reflect low structural dimensionality. Both compounds exhibit anisotropic conductivity; **1c** has been previously characterized as a low temperature one-dimensional Heisenberg chain in which the spin localization on each dimer alternates along the chain, and **1d** exhibits a similar $S = {}^1/_2$ antiferromagnet state down to approximately 10 K.[26] These reports are consistent with the one-dimensional LDOS observed for each compound in the STM data.

Concluding Remarks

These studies clearly demonstrate that STM can provide highly resolved images of the crystal faces of crystalline 1–D organic charge-transfer conductors. The large molecularly flat crystal faces are indicative of stable low-energy planes, which are a consequence of strong intermolecular bonding (i.e., π–π charge-transfer interactions

(25) (a) Monoclinic: Schwerdtfeger, C. F.; Oostra, S.; Visser, R. J. J.; Sawatzky, G. A. *Solid State Commun.* **1981**, *39*, 1133. (b) Triclinic: Kramer, G. J.; Brom, H. B. *J. Phys. C: Solid State Phys.* **1988**, *21*, 5435. (c) Triclinic: Korving, W. H.; Brom, H. B.; De Jongh, L. J.; Oostra, S.; DeBoer, J. L. *Physica B* **1988**, *153*, 66.

along the stacking direction and van der Waals interactions between the stacks) *within* these planes, and their minimal molecular corrugation. STM can resolve different electronic subsystems associated with crystallographically inequivalent TCNQ *layers*, similar to previous observations of crystallographically inequivalent TCNQ *stacks* in a single layer. A comparison of the measured STM parameters with the X-ray values demonstrates a general agreement between the surface and bulk structure. However, in some crystals the STM lattice parameters are smaller than those expected based on the bulk crystal structure, suggesting compression of the exposed surface layer. This can be attributed to weak interactions normal to the layers, which allows the surface layer to contract and lower its free energy. It is interesting to speculate on whether such surface reconstruction may influence crystal growth, particularly since the macroscopic habit and nanoscale topography observed here reflect slow growth normal to these faces.

The tunneling current contrast observed for the exposed faces of these salts is consistent with the presence of $(TCNQ)_2^-$ dimers or their associated cations. The presence of $(TCNQ)_2^-$ dimers is consistent with the crystal structure of these salts, which reveal dimerized TCNQ stacks. Furthermore, the semiconducting properties, magnetic susceptibility and electron paramagnetic resonance of the $(MORPH)^+(TCNQ)_2^-$ and $(VIN)^+(TCNQ)_2^-$ salts are consistent with contributions from $4k_F$ states at room temperature, which are a consequence of dimerized stacks containing $(TCNQ)_2^-$ dimers.[27] The tunneling current contrast will depend upon the nature of the electronic states near the top of the valence band (for positive tip biases) or near the bottom of the conduction band (for negative tip biases). The negative tip biases used in these studies implicate states near the bottom of the conduction band. Extended Hückel calculations indicate that the TCNQ LUMO has significant contributions to the electron density from the methylidene carbon (fractional spin density $\delta = 0.19$ and 0.11) atoms with smaller contributions arising from the cyano nitrogen atoms ($\delta = 0.04$) and the ring carbon atoms ($\delta = 0.06$).[13a,28] Due to the semiconducting properties of these materials, which is indicative of localized electronic structure, it is reasonable to interpret $\rho(r,E_F)$ of $(MORPH)^+(TCNQ)_2^-$ and $(VIN)^+(TCNQ)_2^-$ salts based on a tight-binding approximation using the partially occupied LUMOs of the TCNQ molecules as the basis, with the largest electronic contribution from the methylidene carbon atoms. For the $4k_F$ structure of the $\rho = 0.5-$ charge-transfer salts, these states feature nodes between TCNQ dimers, at intervals commensurate with the stacking axis.[13a] However, the tunneling current contrast for layers terminated with morpholinium and vinamidinium cations will differ substantially as these cations are closed shell species which are not likely to possess states in the vicinity of E_F. This is supported by comparison of the electrochemical redox potentials of these two species ($E°_{TCNQ/TCNQ^-} = +0.19$ V vs SCE in acetonitrile whereas the dications are not oxidized or reduced within the solvent limits of -2.0 to $+2.0$ V vs SCE). This is evident in the STM data for **1c**.

In summary, these studies demonstrate the capability of STM to distinguish well-defined electronic subsystems in a single material. One must always exercise caution, however, when interpreting STM data for these salts, as $\rho(r,E_f)$ may not be directly related to the positions of the molecules in the unit cell for one-dimensional semiconductors in which the Fermi surface has collapsed to a single point. However, the good agreement of the STM data with the structural and electronic characteristics of the TCNQ layers in these charge-transfer salts strongly support the assignments given. The observation of tunneling current on the layered surfaces indicates that electron transfer to TCNQ molecules at these faces is feasible and can account for crystal growth during electrocrystallization. Further, the molecular level STM characterization provided by studies and the observation of relatively defect-free surfaces with molecular flatness over large areas suggests a potential for these materials as substrates for nucleation studies and nanoscale STM-assisted modification.

Acknowledgment. The authors wish to acknowledge the generous support of the National Science Foundation (NSF/DMR-9107179) and the NSF Center for Interfacial Engineering (NSF Engineering Research Centers Program, CDR 8721551).

(26) (a) Schwerdtfeger, C. F.; Wagner, H. J.; Sawatzky, G. A. *Solid State Commun.* **1980**, *35*, 7. (b) Schwerdtfeger, C. F.; Oostra, S.; Sawatzky, G. A. *Phys. Rev. B* **1982**, *25*, 1786.

(27) (a) Berlinsky, A. J.; Carolan, J. F. *Solid State Commun.* **1974**, *15*, 795. (b) Lowe, J. P. *J. Am. Chem. Soc.* **1980**, *102*, 1262.